

# Structure of the A Site of *Escherichia coli* 16S Ribosomal RNA Complexed with an Aminoglycoside Antibiotic

Dominique Fourmy, Michael I. Recht, Scott C. Blanchard, Joseph D. Puglisi\*

Aminoglycoside antibiotics that bind to 30S ribosomal A-site RNA cause misreading of the genetic code and inhibit translocation. The aminoglycoside antibiotic paromomycin binds specifically to an RNA oligonucleotide that contains the 30S subunit A site, and the solution structure of the RNA-paromomycin complex was determined by nuclear magnetic resonance spectroscopy. The antibiotic binds in the major groove of the model A-site RNA within a pocket created by an A-A base pair and a single bulged adenine. Specific interactions occur between aminoglycoside chemical groups important for antibiotic activity and conserved nucleotides in the RNA. The structure explains binding of diverse aminoglycosides to the ribosome, their specific activity against prokaryotic organisms, and various resistance mechanisms, and provides insight into ribosome function.

Translational accuracy requires specific interaction between aminoacyl-tRNA anticodons and messenger RNA codons, which occurs on the small 30S ribosomal subunit. A highly conserved ribosomal RNA (rRNA) sequence (1), implicated in the maintenance of fidelity, forms the site of the interaction between the codon and the aminoacyl-tRNA anticodon (A site) (Fig. 1A). Structurally related antibiotics, the aminoglycosides (Fig. 2, A and B), bind to this region of rRNA (2) and interfere with protein synthesis by inducing codon misreading (3). Although the precise mechanism of aminoglycoside-induced miscoding is unknown, the antibiotics decrease the dissociation rate of cognate and near cognate aminoacyl tRNA from the A site (4). Resistance enzymes that modify the antibiotic (5) or rRNA (6) have compromised the clinical utility of these antibiotics. To address how aminoglycoside antibiotics bind to rRNA and interfere with translation, we studied the interaction of the aminoglycoside antibiotic paromomycin with an oligonucleotide encompassing the highly conserved A site of 16S rRNA (7). Our analysis of the nuclear magnetic resonance (NMR) structure of the paromomycin-RNA oligonucleotide complex, which we describe below, reveals how aminoglycoside antibiotics bind to the ribosome.

A 27-nucleotide (nt) RNA was used to characterize the structure and antibiotic binding of the small subunit ribosomal A

site (Fig. 1B). Previous work had demonstrated that aminoglycosides bind specifically to a larger, 64-nt RNA that contained the A site (8). Paromomycin binds to the 27-nt oligonucleotide specifically and in a similar way that it binds to the ribosome (Fig. 1, A and B) with the same affinity ( $K_d$ ,  $\sim 10^{-6}$  M) (7). Critical nucleotides for paromomycin binding to the A site include the C<sup>1407</sup> · G<sup>1494</sup> base pair, A<sup>1408</sup>, A<sup>1493</sup>, and U<sup>1495</sup> (Fig. 1C). Base pairing in the lower stem and asymmetry of the internal loop resulting from the presence of a nucleotide at position 1492 are also required for specific binding (7).

In the absence of antibiotic, the internal loop of the A-site oligonucleotide is closed by formation of the base pairs U<sup>1406</sup> · U<sup>1495</sup> and C<sup>1407</sup> · G<sup>1494</sup>. These additional pairs form in the context of a longer oligonucleotide that contains only two G · C pairs in the upper stem (9). A<sup>1408</sup> is stacked within the helix, as are A<sup>1492</sup> and A<sup>1493</sup>. The structure of the internal loop in the region of the three adenines is dynamic, as indicated by mixed sugar conformations, and is not affected by the presence of  $\leq 10$  mM Mg<sup>2+</sup>. The -UUCG- tetraloop forms its previously described structure (10).

After the 1:1 complex of paromomycin and RNA was formed, the solution structure was solved by NMR (11). We obtained (i) 392 NOE (nuclear Overhauser effect)-derived distance restraints (12), which included 47 intermolecular RNA-antibiotic restraints (Fig. 3) (13), and (ii) 154 dihedral torsion restraints (14). Statistics for the 20 final simulated annealing structures (Fig. 4A) (15) are listed in Table 1. The structure of the RNA-paromomycin complex in the region of antibiotic-RNA interaction is well defined; the atomic root-mean-square deviation (rmsd) of the superimposed core

of the 20 final structures is 0.61 Å. The overall definition of the structure is not as good (rmsd 1.52 Å) because long-range features of the RNA, such as groove width and the relative orientations of the two stems, are not well defined by the set of short-range structural restraints (10).

The RNA structure in the complex is essentially two continuous A-form helical stems closing the asymmetric internal loop, which contains noncanonical pairings (Figs. 4B and 5). As in the unbound form, the upper stem is extended through a non-canonical U<sup>1406</sup> · U<sup>1495</sup> base pair and the C<sup>1407</sup> · G<sup>1494</sup> base pair closing the internal loop. The N3 and O4 of U<sup>1406</sup> hydrogen bond with O2 and N3 of U<sup>1495</sup> to form the U<sup>1406</sup> · U<sup>1495</sup> pair, as observed in a crystal structure of an RNA oligonucleotide (16).

Binding of paromomycin stabilizes a distinct structure for the three adenines in the internal loop (A<sup>1408</sup>, A<sup>1492</sup>, A<sup>1493</sup>). Stacked between the two stems and base paired are A<sup>1408</sup> and A<sup>1493</sup> (Fig. 5) (17). The A<sup>1408</sup> N6-A<sup>1493</sup> N7 and A<sup>1408</sup> N1-A<sup>1493</sup> N6 distances in the ensemble of structures are  $4.0 \pm 0.1$  Å and  $3.7 \pm 0.1$  Å, values consistent with direct or water-mediated hydrogen-bond formation. The

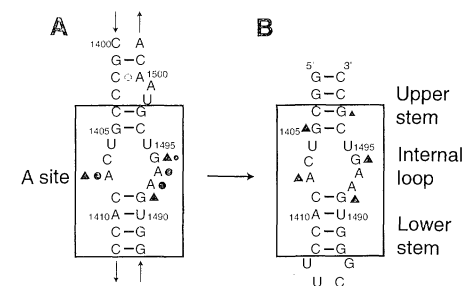


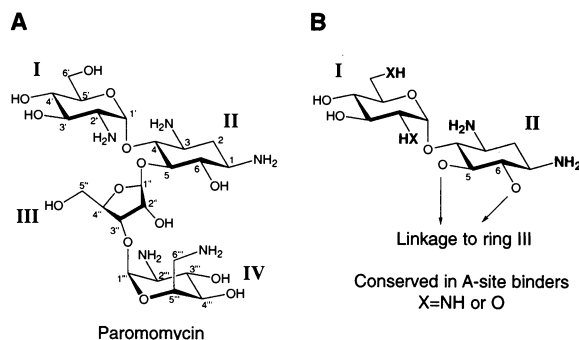
**Fig. 1.** (A) The secondary structure of *E. coli* 16S RNA in the region of the A site. Base pairs that form on the basis of phylogenetic comparison of mitochondrial sequences are indicated. (●) Nucleotides protected from chemical probes by A-site tRNA bound to 30S subunits. (▲) Nucleotides protected from chemical probes by aminoglycoside antibiotics bound to 30S subunits. (B) Sequence of the A-site model oligonucleotide, showing nucleotides present in 16S ribosomal RNA (boxed), and stem and loop regions. (▲) Nucleotides in the model that are protected from reaction with chemical probes in the presence of aminoglycoside antibiotics. (C) RNA sequence elements critical for specific aminoglycoside binding to the A-site RNA oligonucleotide. Required nucleotides are shown explicitly; N, any nucleotide; N-N, any Watson-Crick base pair. For position 1495, either a U or G gives high affinity binding, and each presents a hydrogen bond acceptor in the major groove.

D. Fourmy, S. C. Blanchard, J. D. Puglisi, Department of Chemistry and Biochemistry, Center for Molecular Biology of RNA, University of California, Santa Cruz, CA 95064, USA.

M. I. Recht, Department of Biology, Center for Molecular Biology of RNA, University of California, Santa Cruz, CA 95064, USA.

\*To whom correspondence should be addressed.

**Fig. 2.** Chemical structures for aminoglycoside antibiotics. **(A)** Paromomycin; for neomycin, the 6'-OH is replaced by an amino group. **(B)** Conserved structural elements within all aminoglycoside antibiotics that bind to the ribosomal A site. I, II, III, and IV signify ring numbering.



$A^{1408}$ - $A^{1493}$  pair is buckled in the ensemble of conformations, with  $A^{1493}$  at a  $45^\circ$  angle to the plane of  $A^{1408}$ . Formation of the  $A^{1408}$ - $A^{1493}$  pair is consistent with protection of the N1 position of  $A^{1408}$  from methylation upon binding of paromomycin to the ribosome and A-site oligonucleotide. The reactivities of the N1 positions of  $A^{1492}$  and  $A^{1493}$  are unaffected by antibiotic binding, and these groups are solvent accessible on the minor groove side in the antibiotic-RNA complex. The RNA backbone is distorted by the presence of the bulged nucleotide  $A^{1492}$  and noncanonical  $A^{1408}$ - $A^{1493}$  pair. This distortion arises from nonstandard values of backbone dihedral torsion angles (17) and leads to formation of a distinct binding pocket for paromomycin.

Paromomycin binds in the major groove of the A-site RNA within the internal loop (Fig. 4B). Paromomycin in solution has rather rigid ring conformations (18), but is flexible about the glycosidic linkages connecting the rings. Bound to the RNA, the antibiotic adopts an L-shaped conformation. Rings II, III, and IV form a linear array that lines the major groove from the  $U^{1406}$ - $U^{1495}$  base pair to the  $A^{1410}$ - $U^{1490}$  base pair. Ring IV is partially disordered (Table 1) in the ensemble of 20 structures. Ring I is positioned near the  $A^{1408}$ - $A^{1493}$  pair and  $A^{1492}$  at approximately a  $90^\circ$  angle to rings II, III, and IV. Rings I and II adopt chair conformations, with the amino and hydroxyl substituents in equatorial positions, and these exocyclic groups make specific contacts that stabilize the antibiotic-RNA complex (Fig. 6). The binding site of the antibiotic is consistent with the protections from reactivity with dimethyl sulfate observed on complex formation in the ribosome and A-site oligonucleotide.

Ring II (2-deoxystreptamine) spans the  $U^{1406}$ - $U^{1495}$  and  $C^{1407}$ - $G^{1494}$  base pairs. The amino groups at positions 1 and 3 of ring II make hydrogen bonds to the O4 of  $U^{1495}$  and the N7 of  $G^{1494}$ , respectively. The amino group at position 3 may also make contact with the phosphate between  $A^{1493}$  and  $G^{1494}$ . The  $C^{1407}$ - $G^{1494}$  base

pair is required for specific aminoglycoside binding (7), and carboxyethylation of the N7 position of  $G^{1494}$  interferes with paromomycin binding (19). The presence of a hydrogen bond acceptor in the major groove at position 1495 is essential for specific binding (7). The  $U^{1406}$ - $U^{1495}$  and  $C^{1407}$ - $G^{1494}$  base pairs, involved in the specific contacts with ring II, are universally conserved in all ribosomes. The two amino groups of ring II, found in all aminoglycosides that bind to the A site (Fig. 2B), are required for specific binding of these antibiotics to ribosomal RNA.

Ring I of paromomycin lies in the pocket that is opened by the bulged nucleotide  $A^{1492}$  and the  $A^{1408}$ - $A^{1493}$  base pair, which are both required for specific complex formation. Ring I stacks above the base moiety of  $G^{1491}$  (Fig. 6) and is surrounded by the phosphate groups of residues  $A^{1492}$  and  $A^{1493}$ . The orientation of the conserved

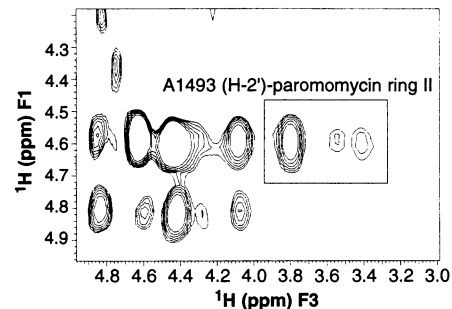


**Fig. 3.** Two-dimensional plane at the chemical shift of  $A^{1493}$  C-2' (75.0 ppm) from a  $F_3$ - $^{13}C$ -filtered three-dimensional  $^{13}C$  HMQC-NOESY experiment performed on the A-site RNA-paromomycin complex at  $35^\circ C$  with a mixing time of 200 ms. Intermolecular NOEs between the proton 2' of  $A^{1493}$  with ring II of paromomycin are boxed.

hydrogen bond donor at the 6' position, -OH in paromomycin, is not well defined in the solution structure. The distance between the ring I C-6' and the pro-R oxygen of the  $A^{1493}$  phosphate ( $4.4 \pm 0.4 \text{ \AA}$ ) is consistent with a direct contact between the 6'-OH function of ring I and the phosphate group of  $A^{1493}$ . The 3'- and 4'-OH groups on ring I are close (3.9 and 3.7  $\text{\AA}$ ) to the  $A^{1493}$  and  $A^{1492}$  phosphates, respectively, but these hydroxyl groups are not essential for aminoglycoside function (20). Replacement of the pro-R oxygens at  $A^{1492}$  and  $A^{1493}$  by a sulfur atom interferes with paromomycin binding (19). The amino group at the 2' position of ring I forms a hydrogen bond with the O4'

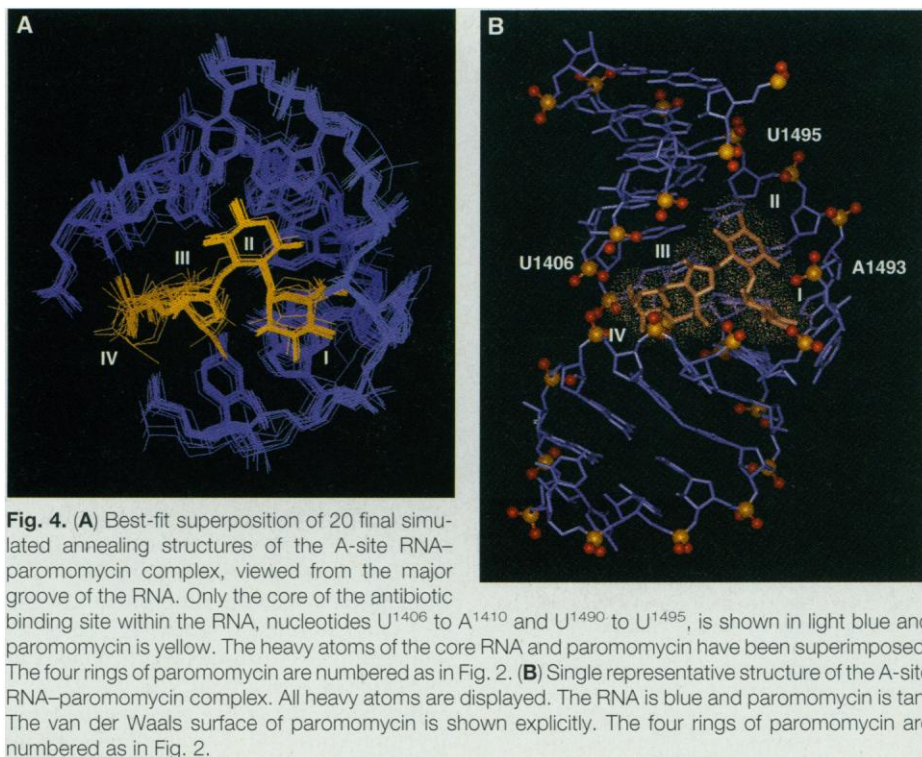


**Fig. 4.** **(A)** Best-fit superposition of 20 final simulated annealing structures of the A-site RNA-paromomycin complex, viewed from the major groove of the RNA. Only the core of the antibiotic binding site within the RNA, nucleotides  $U^{1406}$  to  $A^{1410}$  and  $U^{1490}$  to  $U^{1495}$ , is shown in light blue and paromomycin is shown in yellow. The heavy atoms of the core RNA and paromomycin have been superimposed. The four rings of paromomycin are numbered as in Fig. 2. **(B)** Single representative structure of the A-site RNA-paromomycin complex. All heavy atoms are displayed. The RNA is blue and paromomycin is tan. The van der Waals surface of paromomycin is shown explicitly. The four rings of paromomycin are numbered as in Fig. 2.

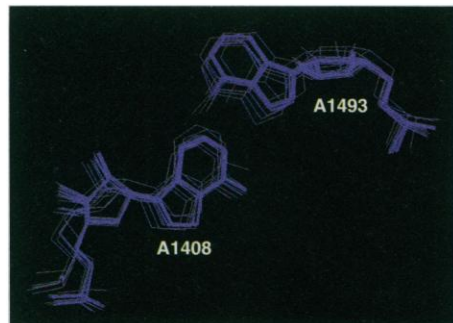


**Fig. 5.** The A<sup>1408</sup>-A<sup>1493</sup> base pair. Superposition of the 20 final structures of the RNA-paromomycin complex, viewed down the helix axis from the upper stem.

atom in ring III. This internal hydrogen bond in paromomycin may help to orient ring I for specific binding with the RNA.

The antibiotic-RNA interaction is extended along the major groove by rings III and IV. The amino and hydroxyl groups of ring IV make probable electrostatic contacts with the phosphate backbone at U<sup>1406</sup>, C<sup>1407</sup>, and U<sup>1490</sup>. High affinity aminoglycoside binding to the A site requires base pairing in the lower stem, but it is relatively independent of nucleotide sequence. Sequence-independent interaction of positively charged ligands, such as spermine, has been observed in the major groove of RNA helices (21). Rings III and IV contribute weakly to specific antibiotic binding and function in that similar complexes are formed with ribostomycin or neamine, two neomycin-related antibiotics that lack ring IV and both rings III and IV, respectively (7).

Aminoglycoside antibiotics act preferentially on prokaryotic organisms. Prokaryotic ribosomes are sensitive to a 10 to 15 times lower antibiotic concentration than are eukaryotic ribosomes (22). Prokaryotic rRNA sequences have an A at position 1408, whereas in eukaryotic sequences this position is a G. The A<sup>1408</sup>-A<sup>1493</sup> pair is essential for antibiotic binding, and leads to formation of the specific binding pocket for ring I. A base pair of equivalent geometry cannot be formed with the eukaryotic G<sup>1408</sup>-A<sup>1493</sup> configuration, and paromomycin binds weakly to a G<sup>1408</sup> variant oligonucleotide (7). A base pair at the 1409 and 1491 positions provides the floor of the antibiotic binding pocket (Fig. 7), and its disruption leads to aminoglycoside resistance in prokaryotes (23). Higher eukaryotic organisms, including humans, have cytoplasmic rRNA sequences containing both disruptions: G<sup>1408</sup> and a mispair at the 1409-1491 positions (by the *Escherichia coli* numbering system), and thus their ribosomes cannot bind aminoglycoside anti-

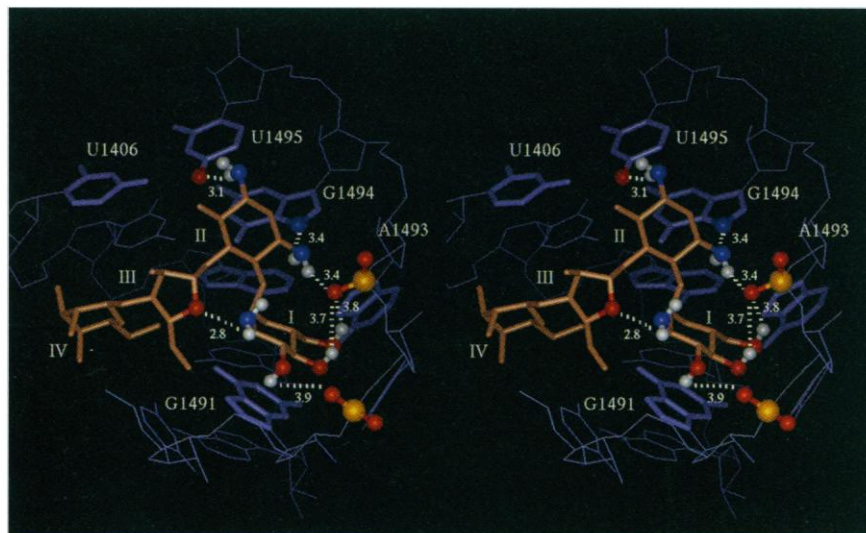


**Fig. 6.** Stereo view of specific contacts made between rings I and II of paromomycin and A-site RNA. The RNA is in blue, paromomycin is tan, and the view is into the major groove of the RNA core. The U<sup>1406</sup>-U<sup>1495</sup>, A<sup>1408</sup>-A<sup>1493</sup> base pairs, as well as G<sup>1494</sup> and G<sup>1491</sup>, are highlighted in the structure. Possible hydrogen bonding contacts are indicated by dashed lines. The distances represent the average heavy atom distance within the collection of 20 final structures.

otics with high affinity.

Enzymatic methylation of rRNA residues A<sup>1408</sup> or G<sup>1405</sup> at the N1 and N7 positions, respectively, results in resistance to specific combinations of aminoglycosides (6) (Fig. 7). Methylation at A<sup>1408</sup>(N1), a hydrogen bond acceptor in the A<sup>1408</sup>-A<sup>1493</sup> base pair, prevents formation of this essential base pair for the aminoglycoside binding and leads to kanamycin resistance. Methylation at G<sup>1405</sup>(N7) confers resistance to kanamycin and gentamicin, in which ring III is linked to position 6 in ring II. Initial NMR evidence places ring III of gentamicin in proximity to G<sup>1405</sup> (24), and the resulting steric clash upon methylation could explain the specific resistance observed for this subclass of aminoglycosides. The natural 5-methyl modification of C<sup>1407</sup> in *E. coli* 16S rRNA was modeled in the structure of the A-site oligonucleotide-paromomycin complex with no distortion.

The enzymatic modification of aminoglycosides is the predominant resistance mechanism to this class of antibiotics (5). Modification enzymes primarily target rings I and II, which direct specific interaction with the A site (Fig. 7). Enzymatic acetylation of the conserved amino group on ring II (position 3) would disrupt the hydrogen bond involving this amino function and the N7 of G<sup>1494</sup>, as well as specific electrostatic and hydrogen bonding contacts with A<sup>1493</sup> phosphate. A 6'-amino group on ring I can be acetylated, giving rise to aminoglycoside resistance. Ring I fits tightly in a pocket and modification at this position may prevent binding by steric hindrance (Fig. 7). Phos-

phorylation and adenylation of the 3'- and 4'-OH, respectively, in ring I would lead to steric and electrostatic penalties to complex formation.

Aminoglycosides that bind in the A site can form the same set of specific RNA-antibiotic interactions observed in the paromomycin-RNA complex. The ef-

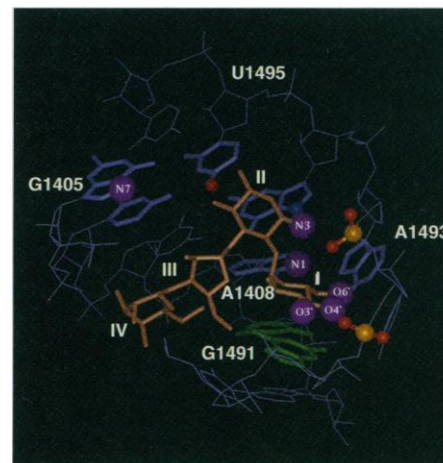


**Fig. 7.** Sites of covalent modifications to A-site rRNA and antibiotic that lead to aminoglycoside resistance. The RNA is blue and paromomycin is tan. G<sup>1405</sup>, U<sup>1406</sup>-U<sup>1495</sup>, A<sup>1408</sup>-A<sup>1493</sup>, and G<sup>1494</sup> are highlighted in blue, and chemical groups in the rRNA that are involved in specific contacts are shown explicitly. The sites of action of aminoglycoside modification enzymes (ring I O3', O4', O6', ring II, N3) and RNA methylases (G<sup>1405</sup>, N7; A<sup>1408</sup>, N1) are shown as purple spheres on the aminoglycoside and RNA, respectively. The C<sup>1409</sup>-G<sup>1491</sup> base pair, whose disruption leads to aminoglycoside resistance, is highlighted in green.

ficacy of later generation aminoglycosides, such as amikacin, tobramycin, and the gentamicins are related to the structural features described above. In amikacin, position 1 of ring II is substituted by a bulky chain [NH-CO-CH(OH)-CH<sub>2</sub>-CH<sub>2</sub>-NH<sub>2</sub>]. The NH can form a hydrogen bond with the O4 of U<sup>1495</sup> and the long chain could exit the major groove without affecting A-site binding but, at the same time, block resistance enzymes that modify ring II. Tobramycin and certain gentamicins lack 3'- and 4'-OH groups in ring I that are targeted by resistance enzymes, but do not contribute to specific complex formation. The paromomycin-RNA structure can be used to design novel aminoglycoside antibiotics.

Our paromomycin-A-site RNA structure suggests an origin for aminoglycoside antibiotic-induced miscoding. The ribosome contributes to specific reading of the genetic code, as Watson-Crick base pairing between anticodon and codon is insufficient to account for the fidelity of translation (25, 26). Factors, such as binding of aminoglycoside antibiotics, that decrease dissociation rates of aminoacyl-tRNA inhibit translational processivity and favor miscoding by affecting a proofreading branchpoint (4). Aminoglycosides may stabilize a high affinity conformation of rRNA for the tRNA-mRNA complex.

Specific binding of the conserved rings I and II, within the neomycin-related aminoglycosides, locks the dynamic residues A<sup>1492</sup> and A<sup>1493</sup> of the RNA in a unique conformation.

The ribosome must sense formation of the codon-anticodon interaction through structure-specific, sequence-independent interactions. The N1 positions of the universally conserved A<sup>1492</sup> and A<sup>1493</sup>, which point into the minor groove in the A-site RNA-paromomycin structure, could contact two 2'-OH groups in the mRNA that are presented in a helical conformation when a cognate tRNA binds the correct codon. A<sup>1492</sup> and A<sup>1493</sup> are protected at the N1 position by mRNA-dependent tRNA binding to the ribosome (1) and substitution of deoxynucleotides in the A-site codon of mRNA decreases the affinity of A-site tRNA binding (27). Similar adenine N1-helical 2'-OH interactions occur in the core of the group I intron (28). The interactions between adenine N1 and 2'-OH could represent an initial step in communication between a codon-anticodon complex, and the guanosine triphosphatase site of EF-Tu (29), located on the large subunit.

The structure of the paromomycin-RNA complex shows how therapeutic agents can target RNA structures. In that antibiotics interfere with essential ribosome functions,

structural studies on antibiotic-rRNA interactions increase our understanding of these functions.

## REFERENCES AND NOTES

1. D. Moazed and H. F. Noller, *J. Mol. Biol.* **211**, 135 (1990); H. F. Noller, *Annu. Rev. Biochem.* **60**, 191 (1991); R. A. Zimmermann, C. L. Thomas, J. Wower, in *The Ribosome Structure, Function and Evolution*, W. E. Hill *et al.*, Eds. (American Society for Microbiology, Washington, DC, 1990), pp. 331-347.
2. D. Moazed and H. F. Noller, *Nature* **327**, 389 (1987); J. Woodcock, D. Moazed, M. Cannon, J. Davies, H. F. Noller, *EMBO J.* **10**, 3099 (1991).
3. J. Davies and B. D. Davis, *J. Biol. Chem.* **243**, 3312 (1968); P. Edelmann and J. Gallant, *Cell* **10**, 131 (1977); E. F. Gale, E. Cundliffe, P. E. Reynolds, M. H. Richmond, M. J. Waring, *The Molecular Basis of Antibiotic Action* (Wiley, London, 1981).
4. R. Karimi and M. Ehrenberg, *Eur. J. Biochem.* **226**, 355 (1994).
5. K. J. Shaw, P. N. Rather, R. S. Hare, G. H. Miller, *Microbiol. Rev.* **57**, 138 (1993).
6. A. A. D. Beauclerk and E. Cundliffe, *J. Mol. Biol.* **193**, 661 (1987).
7. M. I. Recht, D. Fourmy, S. C. Blanchard, K. D. Dahlquist, J. D. Puglisi, *J. Mol. Biol.* **262**, 421 (1996).
8. P. Purohit and S. Stern, *Nature* **370**, 659 (1994).
9. D. Fourmy and J. D. Puglisi, unpublished results. A 43-nt RNA had a similar structure in the A site as determined by NMR.
10. F. H.-T. Allain and G. Varani, *J. Mol. Biol.* **250**, 333 (1995).
11. Milligram quantities of the 27-nt A-site RNA were prepared unlabeled, uniformly <sup>13</sup>C-labeled, or with adenines specifically <sup>13</sup>C- and <sup>15</sup>N-labeled by transcription with T7 RNA polymerase [J. D. Puglisi and J. R. Wyatt, *Methods Enzymol.* **261**, 323 (1995)]. All NMR experiments were recorded on a Varian Unity+ 500 MHz spectrometer equipped with triple resonance, z-gradient probes. NMR experiments were performed in 10 mM sodium phosphate (pH 6.4 or 5.5), primarily at 35°C. The concentrations of unlabeled RNA, uniformly <sup>13</sup>C-labeled RNA, and specifically <sup>15</sup>N-, <sup>13</sup>C-labeled RNA were 4.5 mM, 3 mM, and 3 mM, respectively. Exchangeable and nonexchangeable protons of the paromomycin were partially assigned by means of standard NMR experiments. The assignment of the nonexchangeable protons of the labeled RNA and paromomycin was completed with the use of constant-time HSQC [J. Santoro and G. King, *J. Magn. Res.* **97**, 202 (1992)], 3D-HCCH-TOCSY, 3D-HMQC-NOESY [G. M. Clore *et al.*, *Biochemistry* **29**, 8172 (1990)] and <sup>13</sup>C-filtered NOESY and TOCSY [G. Otting and K. Wüthrich, *Q. Rev. Biophys.* **23**, 39 (1990); W. Lee *et al.*, *FEBS Lett.* **350**, 87 (1994)]. Sequential connectivities between nucleotides in RNA were obtained by HP-COSY and HCP. Adenine H2 protons were assigned by correlation to H8 resonances by 2D HCCH-TOCSY [J. P. Marino *et al.*, *J. Am. Chem. Soc.* **116**, 2205 (1994)]. The hydrogen bonding patterns of the base pairs were determined from analysis of SSNOESY spectra in water at different mixing times (75, 150, and 300 ms) [S. H. Smallcombe, *J. Am. Chem. Soc.* **115**, 4776 (1993)]. For the U-U base pair a strong NOE was observed between the two imino protons.
12. Distance restraints for nonexchangeable RNA protons were derived from visual inspection of NOESY cross-peak intensities at 50, 100, 150, 200, and 250 ms NOESY. NOEs were classified into three distance bound ranges: strong 1.8 to 2.5 Å, medium 2.5 to 3.5 Å, and weak 3.5 to 5 Å (or 3.5 to 5.5 Å for some NOEs with exchangeable protons of the RNA, obtained from 75- and 150-ms SSNOESY experiments, or 3.5 to 6 Å for some intermolecular NOEs involving dynamic rings of the paromomycin). Appropriate pseudoatom distance corrections were used.
13. Paromomycin-RNA NOE restraints in structure calculations included U<sup>1406</sup>(H5)-ring IV(1'', 2''),

**Table 1.** Structural statistics and atomic root-mean-square (rms) deviations.

Item	⟨SA⟩*	(SA)r	⟨SA⟩	
			Versus SA	Versus (SA)r
Final forcing energies distance and dihedral restraints (kcal · mol <sup>-1</sup> )	38 ± 10	47		
rms deviation from experimental distance restraints (Å)†				
All (392)	0.0396 ± 0.0023	0.0400		
RNA (332)	0.0349 ± 0.0016	0.0362		
Paromomycin (13)	0.0736 ± 0.0136	0.0762		
RNA-paromomycin (47)	0.0545 ± 0.0088	0.0509		
rms deviation from experimental dihedral restraints (degrees) (154)	0.0260 ± 0.0122	0.0850		
Deviations from idealized geometry				
Bonds (Å)	0.0256 ± 0.0001	0.0257		
Angles (degrees)	0.0630 ± 0.0007	0.0634		
Improper (degrees)	0.0834 ± 0.0158	0.0536		
Heavy-atom rms deviation (Å)				
All RNA + paromomycin			1.52	1.82
Ordered RNA + paromomycin‡			0.61	0.77
Paromomycin			0.59	0.61
Paromomycin ring I			0.24	0.34
Paromomycin ring II			0.03	0.04
Paromomycin ring III			0.36	0.38
Paromomycin ring IV			0.48	0.40

\*⟨SA⟩ refers to the final 20 simulated annealing structures, SA to the average structure obtained by taking the average coordinates of the 20 simulated annealing structures best-fitted to one another, and (SA)r to the average structure after restrained energy minimization. †Two structures each contained one 0.3 to 0.35 Å distance violation, and except for these violations the 20 final structures did not contain distance violations of >0.25 Å or dihedral violations of >20°. Numbers in parentheses refer to number of restraints. ‡RNA residues 1406 to 1410, 1490 to 1495, and all paromomycin residues.

- U<sup>1406</sup>(H3)-ring II(6), U<sup>1406</sup>(H6)-ring IV(4''), C<sup>1407</sup>(H4)-ring II(6), ring III(2''), C<sup>1407</sup>(H5)-ring IV(1'', 2''), A<sup>1408</sup>(H6)-ring I(1') ring II(6), G<sup>1499</sup>(H8)-ring IV(4''), U<sup>1490</sup>(H5)-ring III(3', 4', 5') ring IV(3'', 4'', 5'', 6''), U<sup>1490</sup>(H6)-ring II(5''), G<sup>1491</sup>(H1)-ring I(1'), G<sup>1491</sup>(H2')-ring I(3', 4'), G<sup>1491</sup>(H3')-ring II(2', 3'), A<sup>1492</sup>(H3')-ring I(3', 4', 5'), A<sup>1492</sup>(H5')-ring I(3'), A<sup>1493</sup>(H2')-ring II(3), A<sup>1493</sup>(H3')-ring II(2 equatorial, 3), A<sup>1493</sup>(H5')-ring II(3), A<sup>1493</sup>(H8)-ring I(3', 4', 5') ring II(2 axial), G<sup>1494</sup>(H1)-ring II(2 axial, 2 equatorial, 6), G<sup>1494</sup>(H3')-ring II(2 axial, 2 equatorial), U<sup>1495</sup>(H5)-ring II(1, 2 axial, 2 equatorial, 3, 6), U<sup>1495</sup>(H3)-ring II(6).
14. RNA dihedral restraints were assigned following the general strategy of Varani and co-workers [F. H.-T. Allain and G. Varani, *J. Mol. Biol.* **250**, 333 (1995)].  $\beta$ -Dihedral angles were restrained from estimates of the  $^3J_{P-H5'}$ ,  $^3J_{P-H5''}$ , and  $^3J_{P-C4'}$  coupling constants from the HP-COSY and HCP experiments [J. P. Marino *et al.*, *J. Am. Chem. Soc.* **116**, 6472 (1994)]. When evidence for a trans  $\beta$  angle was observed, this angle was restrained to  $180 \pm 30^\circ$ .  $\epsilon$  was restrained from estimates of  $^3J_{H3'-P}$ ,  $^3J_{C2'-P}$ , and  $^3J_{C4'-P}$  from HP-COSY and HCP. Constraints of  $210 \pm 30^\circ$  (trans) or  $260 \pm 30^\circ$  (gauche<sup>-</sup>) or  $235 \pm 55^\circ$  (when the trans or gauche<sup>-</sup> conformations could not be distinguished) were used. The  $\gamma$  dihedral angles were constrained from estimates of  $^3J_{H4'-H5'}$  and  $^3J_{H4'-H5''}$  coupling constants from the <sup>31</sup>P decoupled DQF-COSY and the 3D HMQC-TOCSY experiment with a short (20 ms) mixing time. For a gauche<sup>+</sup> conformation,  $\gamma$  was constrained to  $55 \pm 30^\circ$  (or  $\pm 40^\circ$ ). The ribose sugar pucker was estimated from analysis of  $^3J_{H1'-H2'}$  in the <sup>31</sup>P decoupled DQF-COSY spectrum. Ribose conformation was restrained to C<sub>2'</sub>-endo ( $\delta = 160 \pm 30^\circ$ ) or C<sub>3'</sub>-endo ( $\delta = 85 \pm 30^\circ$ ) when  $^3J_{H1'-H2'}$  was  $>8$  Hz or  $<3$  Hz, respectively. No restraints were used for riboses with mixed sugar conformations. Several paromomycin ring I and II dihedral angles were restrained from analysis of the short mixing time TOCSY and DQF-COSY spectrum.
15. Structures were calculated using a simulated annealing protocol within the InsightII NMRArchitect package (Biosym Technologies, San Diego, CA). A randomized array of atoms corresponding to RNA and paromomycin was heated to 1000 K, and bonding, distance and dihedral restraints, and a repulsive quartic potential were gradually increased to full value over 40 ps of molecular dynamics. The molecules were then cooled during 10 ps to 300 K and subjected to a final energy minimization step that included an attractive Lennard-Jones potential. No electrostatic term was included in the target function. Using this protocol, 30% of the structures converged, as based on restraint violation energies, and 30 of them were collected to be further refined with the final set of restraints. There were differences of greater than  $100 \text{ kcal} \cdot \text{mol}^{-1}$  between converged and unconverged structures. During refinement, molecules were heated to 1000 K and subject to 30 ps of molecular dynamics following the same protocol as above. The molecules were then cooled during 10 ps to 300 K and subjected to a final energy minimization step that again included an attractive Lennard-Jones potential and no electrostatic term. A total of 392 distance restraints were used including 91 intranucleotide RNA restraints, 198 internucleotide RNA, 43 base pair hydrogen bonding restraints, 13 interresidue paromomycin restraints, and 47 RNA-paromomycin restraints; no hydrogen bonding restraints were used for non-canonical base pairs. A total of 154 experimental dihedral restraints were used, comprising 8 paromomycin and 146 RNA restraints. Additional restraints were used to maintain chirality, and base pair planarity outside the internal loop of the RNA. The final force constants for distance restraints were  $40 \text{ kcal} \cdot \text{mol}^{-1}$ . Base pairing hydrogen bond and dihedral restraints final force constants were set to  $60 \text{ kcal} \cdot \text{mol}^{-1}$ . All color figures were generated with the program InsightII (Biosym Technologies, San Diego, CA).
16. K. J. Baeyens, H. L. De Bondt, S. R. Holbrook, *Nature Struct. Biol.* **2**, 56 (1995).
17. The A<sup>1408</sup>-A<sup>1493</sup> pair geometry was defined by distance restraints derived from <sup>15</sup>N-correlated NOESY experiments for exchange-broadened protons [L. Mueller, P. Legault, A. Pardi, *J. Am. Chem. Soc.* **117**, 11043 (1995)] performed on the complex containing specifically <sup>15</sup>N-, <sup>13</sup>C-labeled adenines. Adenine amino nitrogens were assigned by through-bond correlation to H8 and H2 protons after 2D and 3D HNC-TOCSY-CH experiments [J. P. Simorre, G. R. Zimmermann, L. Mueller, A. Pardi, *J. Am. Chem. Soc.* **118**, 5316 (1996)]. The  $\epsilon$  angle for A<sup>1493</sup> adopts a gauche<sup>-</sup> conformation, and the torsion angle  $\alpha$  for the phosphate between G<sup>1491</sup> and A<sup>1492</sup> adopts a trans conformation. The latter is consistent with the downfield chemical shift of the corresponding <sup>31</sup>P resonance, even though this information was not used during calculations.
18. D. G. Reid and K. Gajjar, *J. Biol. Chem.* **262**, 7967 (1987).
19. S. Blanchard and J. D. Puglisi, unpublished results.
20. R. Benveniste and J. Davies, *Antimicrob. Agents Chemother.* **4**, 402 (1973).
21. G. Dirheimer, G. Keith, P. Dumas, E. Westhof, in *tRNA Structure, Biosynthesis, and Function*, D. Söll and U. L. Rajbhandary, Eds. (American Society for Microbiology, Washington, DC, 1995), pp. 93-126.
22. J. M. Wilhelm, S. E. Pettitt, J. J. Jessop, *Biochemistry* **17**, 1143 (1978).
23. E. A. DeStasio, D. Moazed, H. Noller, A. E. Dahlberg, *EMBO J.* **8**, 1213 (1989); E. A. DeStasio and A. E. Dahlberg, *J. Mol. Biol.* **212**, 127 (1990).
24. S. Yoshizawa and J. D. Puglisi, unpublished results.
25. H. J. Grosjean, S. De Henau, D. M. Crothers, *Proc. Natl. Acad. Sci. U.S.A.* **75**, 610 (1978).
26. J. J. Hopfield, *ibid.* **71**, 4135 (1974); J. Ninio, *Biochimie* **57**, 587 (1975).
27. A. P. Patapov, F. J. Triana-alonso, K. Nierhaus, *J. Biol. Chem.* **270**, 17680 (1995).
28. A. M. Pyle and T. R. Cech, *Nature* **350**, 628 (1991); A. M. Pyle, F. L. Murphy, T. R. Cech, *ibid.* **358**, 123 (1992).
29. M. V. Rodnina, T. Pape, R. Fricke, L. Kuhn, W. Wintermeyer, *J. Biol. Chem.* **271**, 646 (1996).
30. We thank H. Noller for encouragement and discussions, A. Pardi for assistance with NMR techniques, E. V. Puglisi for comments and support, and M. Ares and R. Green for reading the manuscript. Supported by grants from the Packard Foundation, the Deafness Research Foundation, National Institute of Health (GM51266-01A1), Lucille P. Markey Charitable Trust (J.D.P.), and a postdoctoral grant from Institut National de la Santé et de la Recherche Médicale (D.F.). The coordinates have been deposited in the Brookhaven Protein Data Bank with access number T9496.

26 April 1996; accepted 13 September 1996

## Major Susceptibility Locus for Prostate Cancer on Chromosome 1 Suggested by a Genome-Wide Search

Jeffrey R. Smith,\* Diha Freije,\* John D. Carpten,\* Henrik Grönberg,\* Jianfeng Xu,\* Sarah D. Isaacs, Michael J. Brownstein, G. Steven Bova, Hong Guo, Pirooska Bujnovszky, Deborah R. Nusskern, Jan-Erik Damber, Anders Bergh, Monika Emanuelsson, Olli P. Kallioniemi, Jennifer Walker-Daniels, Joan E. Bailey-Wilson, Terri H. Beaty, Deborah A. Meyers, Patrick C. Walsh, Francis S. Collins, Jeffrey M. Trent,† William B. Isaacs

Despite its high prevalence, very little is known regarding genetic predisposition to prostate cancer. A genome-wide scan performed in 66 high-risk prostate cancer families has provided evidence of linkage to the long arm of chromosome 1 (1q24-25). Analysis of an additional set of 25 North American and Swedish families with markers in this region resulted in significant evidence of linkage in the combined set of 91 families. The data provide strong evidence of a major prostate cancer susceptibility locus on chromosome 1.

Prostate cancer is the most common malignancy diagnosed in U.S. males, accounting for more than 40,000 deaths in this country annually (1). African Americans have the highest incidence and mortality rates of any population studied (2). Numerous studies have provided evidence for familial clustering of prostate cancer, indicating that family history is a major risk factor for this disease (3-5). Segregation analysis of familial prostate cancer suggests the existence of at least one dominant susceptibility locus and predicts that rare high-risk alleles at such loci account in the aggregate for 9% of all prostate cancers and more than 40% of early onset disease (6).

Analyses of genetic alterations in pros-

tate cancer have demonstrated frequent duplication of DNA sequences on the distal long arm of chromosome 8 (7), as well as loss of DNA sequences resulting in loss of heterozygosity (LOH) for the short arm of chromosome 8 and the long arm of chromosome 13 (8, 9). Preliminary investigations by linkage analysis of these regions as well as sites of known tumor suppressor genes have not identified a susceptibility locus in prostate cancer (10, 11).

Prostate cancer presents a number of serious obstacles to linkage analysis. The prevalence is extremely high; there is a one in five lifetime probability of prostate cancer diagnosis in U.S. males (1). This potentially could